Langmuir

Article

pubs.acs.org/Langmuir

Cation Bridging Studied by Specular Neutron Reflection

Xiaofan Wang,[†] Seung Yeon Lee,[†] Kathryn Miller,[†] Rebecca Welbourn,[†] Isabella Stocker,[†] Stuart Clarke,*[,†] Michael Casford,[‡] Philipp Gutfreund,[§] and Maximilian W. A. Skoda[∥]

[†]BP Institute and Department of Chemistry, University of Cambridge, Cambridge, U.K.

[‡]Department of Chemistry, University of Cambridge, Cambridge, U.K.

[§]Institute Laue Langevin, Grenoble, France

[∥]ISIS, Rutherford Appleton laboratory, Harwell Science and Innovation Campus, Didcot, U.K.

ABSTRACT: The binding of an anionic surfactant onto an anionic surface by addition of divalent ions is reported based on experimental data from specular neutron reflection (NR) and attenuated total internal reflection IR spectroscopy (ATR-IR). Similar measurements using monovalent ions (sodium) do not show any evidence of such adsorption, even though the amount of surfactant can be much higher. This data is interpreted in terms of the so-called bridging mechanism of ion binding.

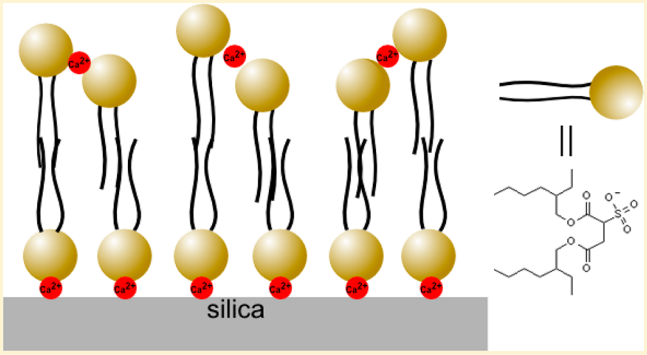

INTRODUCTION

The adsorption of surfactants and other species from solution to solid surfaces underpins many academic and commercially important systems from detergency to oil recovery. There has been a significant amount of work considering the adsorption of cationic or mixed surfactants on anionic surfaces.[1−5] However, the adsorption of charged surfactants on similarly charged surfaces is rather unusual. Indeed, one might expect rather little adsorption due to the electrostatic repulsion between the molecules and the surface. However, in the presence of multivalent ions of opposite charge to the surface and surfactant there have been reports of enhanced adsorption, attributed to the so-called "bridging" effect.

There have been a number of thermodynamic studies of bridging, most particularly for DNA on clays.[6] Thorarinn et al.[7] proposed that the mechanism of cation bridging plays an important role in adsorption of organic matter onto montmorillonite, since the calcium ions enhanced the adsorption, while there was no such enhancement with sodium ions. A number of papers also highlighted the involvement of this mechanism in industrial applications: in particular, Buckley,[8] Lager,[9] and Lee[10] showed this specific ion-binding in application for a crude oil adsorption mechanism. In addition, some surface force measurements[11] have been interpreted as indicating cation bridging—an attractive force has been observed between negatively charged polyacrylate and a like-charged silica surface in the presence of divalent cations over monovalent ones[12,13] and a strong attraction between two negatively charged mineral surfaces in the presence of divalent cations.[14] Attraction has also been observed between negatively charged polymer colloids with divalent ions.[15] Atomic force microscopy was also used to detect an attraction between two silica surfaces upon addition of Co ions[16] and between positively charged colloidal particles with polyanions.[17]

Bridging can also be considered as a two-step process, where the multivalent ions adsorb to one surface reversing its charge and hence making it more attractive to the adsorbing surfactant with the opposite charge. A number of papers emphasized this mechanism by showing the role of multivalent ions as a mediator.[18−27] In addition to this, biomolecules such as DNA and proteins[28−32] were also observed to interact with like-charged surfaces in presence of mutivalent ions.

In this work we report the adsorption of the anionic surfactant aerosol-OT (AOT), sodium bis(2-ethylhexyl) sulfosuccinate, illustrated in Figure 1, onto the surface of a silicon wafer with a native oxide. The surface of the oxide has a number of Si−OH groups that give rise to a pH-dependent surface charge. The isoelectric point for silica is approximately

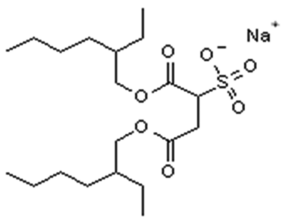

Figure 1. Anionic surfactant aerosol-OT (NaAOT).

Received: February 28, 2013
Revised: April 1, 2013
Published: April 2, 2013

pH = 2,[33−35] and the surface becomes increasingly negative as the pH is increased.[36−39] Hence, over most of the accessible pH range in water both the AOT and silica will be negative (pK_a of AOT = 2[40]). Here we also consider the adsorption of the AOT on the silica in the presence of divalent counterions.

TECHNIQUES

Neutron Reflection. Specular neutron reflection is a powerful technique to study the structure and composition of absorbed species and buried interfaces on molecular scales.[41] The technique involves a highly collimated beam of neutrons impinging onto a very flat surface. In specular reflection, of interest here, the incident angle is equal to the reflected angle (θ), and the scattering is elastic. The reflected intensity is measured as a function of the momentum transfer, Q, normal to the reflecting surface.

$$Q = \frac{4\pi \sin\theta}{\lambda}$$

where λ is the incident neutron wavelength. Neutron reflection can be treated in an analogous way to the reflection of light. The neutron reflective index (n) of nonabsorbing materials can be defined as

$$n = 1 - \frac{\lambda^2 \rho}{2\pi}$$

where ρ is the scattering length density (SLD) of the material and defined by

$$\rho = \frac{\sum b_{coh}}{v_M}$$

where v_M is the molecular volume, b_{coh} is the coherent scattering length of each element present, and the sum is over all atoms in the molecule. The scattering length varies across the periodic table and between isotopes. Typical values of ρ of interest here are given in Table 1.

Table 1. Scattering Length Density of the Compounds Used in This Work[a]

material	formula	$\rho/10^{-6}$ Å^{-2}
silicon	Si	2.07
silicon oxide	SiO_2	3.40
heavy water	D_2O	6.35
water	H_2O	−0.57
contrast-matched water to silicon	D_2O/H_2O	2.07
CaAOT head[a]	$(C_4H_3O_7S)_2Ca$	3.11
CaAOT tail[a]	$(C_{16}H_{34})_2$	−0.40

[a]Note that one Ca^{2+} ion has two AOT anions.

The scattering length density is related to the volume fraction of each component within the layer and is given by

$$\rho = \rho_1\varphi_1 + \rho_2\varphi_2$$

where ρ_1 and ρ_2 are the scattering length density of component 1 and 2, and φ_1 and φ_2 are their volume fractions, where the sum of the volume fractions must be unity (i.e., $\varphi_1 + \varphi_2 = 1$).

Neutrons are effective in characterizing such adsorbed layer systems, particularly when isotopes are used for contrast matching and contrast variation. These allow complicated systems to be simplified dramatically without changing their chemical properties and hence enable one to identify and characterize substrates and any adsorbed layers effectively, highlighting particular regions of interest.

Experimental neutron reflectivity profiles of the different contrasts were simultaneously analyzed using RasCal (version Beta 1, A. Hughes, ISIS Spallation Neutron Source, Rutherford Appleton Laboratory) which employs an optical matrix formalism[42] based on the Abeles method. In this approach the interface is described as a series of slabs, each of which is characterized by its SLD, thickness, and roughness. A least-squares minimization is used to determine the best fit parameters. In all cases the simplest possible model, which adequately described the data, was selected, and all samples under different isotopic contrasts were constrained to be fitted with the same structure (layer and thickness profile) with only the SLD from the different water contrasts varied. Errors on the fitted final values were computed using a bootstrap error estimate method.

Attenuated Total Internal Reflection Infrared (ATR-IR). ATR-IR spectroscopy is a technique used to obtain IR spectroscopic data from a surface immersed in a highly IR absorbing liquid such as water. The IR beam is transmitted through an internal reflection element (IRE) rather than the liquid phase, and hence, little adsorption from the bulk liquid is apparent in a recorded spectra. One advantage of this technique is that the surface sensitivity is enhanced through multiple reflections from the interface at angles below the critical angle. As the IR beam is reflected it gives rise to a standing evanescent wave that extends a short distance into the overlying liquid phase, which decays exponentially with the distance from the IRE with a characteristic length scale, d_p, given by[43−45]

$$d_p = \frac{\lambda}{2\pi n_1\left[\sin^2\theta - \left(\frac{n_2}{n_1}\right)^2\right]^{0.5}}$$

where the refractive index of a sample liquid is n_2 at a wavelength, λ, the refractive index of the internal reflection element, n_1, and the angle of incidence, θ (for example, n of Si crystal = 3.4). This gives rise to an enhanced intensity in the IR spectrum of material close to the IRE surface. For a silicon IRE and an angle of incidence of 60° the penetration depth is typically of the order of 3−4 μm; ATR-IR data therefore contain a contribution from both the bulk solution and the adsorbed layer. In cases where the solution concentration is low and the adsorbed film is comparatively densely packed the observed spectrum is dominated by the adsorbed layer.[46,47] Hence, this approach is ideally suited to the study of adsorbed layers under water where the strong water adsorption bands preclude other IR spectroscopic techniques.

EXPERIMENTAL SECTION

Silicon wafers (55 mm diameter, 5 mm thick, Si (111), N type/P-doped, single side polished, resistivity 1−12 ohm cm) were obtained from CRYSTRAN. Sodium bis(2-ethylhexyl) sulfosuccinate (≥99.0% purity), NaAOT, was purchased from Sigma-Aldrich and used to prepare calcium AOT samples according to the method of Eastoe et al.[48] It should be noted that the exchange reaction of sodium to calcium also changes the stoichiometry from 1:1 (NaAOT) to 2:1 ($Ca(AOT)_2$). In brief the method of exchange includes a liquid−liquid ion-exchange process using a mixture of a saturated calcium nitrate (50 mL, 99.997%, Aldrich) aqueous solution and 1.0 M solution of NaAOT in absolute ethanol (25 mL, >99.8%, Aldrich). This mixture was shaken well and separated with diethyl ether (10 mL, >99.9%, Aldrich). Excess amount of nitrate ion was washed repeatedly with

dx.doi.org/10.1021/la400767u | Langmuir 2013, 29, 5520−5527

water and checked by the brown ring test. The $Ca(AOT)_2$ containing organic upper layer was then evaporated on a rotary evaporator and then left in a vacuum oven at 40 °C for 48 h. NaAOT was purified using the procedure of Li et al.[49] before adsorption.

The silicon wafers were cleaned by mild piranha with a concentration of 5:4:1 of H_2O, concentrated sulfuric acid, and 30% H_2O_2 at temperature near 80 °C for 15 min, followed by extensive rinsing with ultrapure water. Then, the wafers were exposed to UV-ozone for 10 min. All glassware, plastic bottles, other parts of the cell, and connecting tubing were cleaned with Decon 90 followed by extensive rinsing with ultrapure water.

The silicon wafer was clamped against a PTFE trough to make a solid/liquid cell by means of a steel assembly. Solutions were prepared and injected into in the cell manually. The solutions were injected and replaced several times to ensure complete exchange of solutions.

The neutron reflection measurements were made on D17 at the Institute Laue Langevin, Grenoble, France,[50] and INTER at ISIS, the Rutherford Appleton Laboratory.[51] The instruments use either a chopper-shaped pulse of neutrons from the reactor (D17, lambda 2−30 Å) or spallation target (INTER, lambda 1−15 Å) sources. The wavelength is determined by time-of-flight to the detector. For D17 the reflection is collected with the solid/liquid sample in the vertical plane and the incident and reflected beams in the horizontal plane. For INTER, the solid/liquid interface is horizontal and the incident beam is projected down on to the surface and then reflected up. D17 uses a 2D multidetector, and on INTER a single detector is used. Wavelength and scattering angle were used to calculate the appropriate momentum transfer, Q.[50,51] For the 2D detector on D17 the counts can be presented as a function of in-plane scattering angle by summing the counts in columns for each time slice (wavelength). The variation of the reflected signal with wavelength is then obtained for both instruments by normalization to separate transmission measurements straight through the silicon wafer. The beam resolution ($\Delta q/q$) on INTER was 4% and ($\lambda\Delta/\lambda$) 1−7% on D17. The data were analyzed using the software RasCAL.[52]

The solid−liquid cell was mounted on a sample changer on both instruments which were attached to accurate goniometers used to very accurately align the sample and optimize the reflected signal. The measurements were all made at room temperature.

The substrates were initially characterized with three contrasts of water (H_2O, D_2O, and contrast-matched water to silicon (CMWSi)) before exposure to the surfactant solutions with the different metals present as counterions.

Attenuated total reflection infrared (ATR-IR) experiments were performed on a PerkinElmer Spectrum 100 FTIR spectrometer (fitted with a liquid nitrogen cooled mercury cadmium telluride detector) in the Department of Chemistry, University of Cambridge. This device uses a trapezoidal silicon IRE (50 × 20 × 2 mm, CRYSTRAN Ltd.) in a solid/liquid cell. The silicon IREs were cleaned with the same procedures used for the neutron experiments as were the Teflon components of the solid/liquid cell. To avoid the very strong adsorption bands from water perturbing the C−H stretching modes of interest, heavy water (D_2O) was used as the solution phase. To ensure similarity of cleanliness between the neutron and ATR experiments, the usual stainless steel sample container on the ATR was manufactured in PTFE. However, essentially similar results were obtained in both stainless steel and Teflon cells.

RESULTS

The reflectivity profiles of a bare silicon crystal in three contrasts of D_2O, H_2O, and CMWSi are shown in Figure 2. The profiles were fitted with the scattering length density parameters expected for silicon, oxide, D_2O, H_2O, and CMWSi (see Table 1), and very good agreement was found between the expected and experimental data as shown in Figure 2. A surface roughness of 2 ± 1 Å and an oxide layer of 15 ± 3 Å with a roughness of 2 ± 1 Å were included in the model. These values

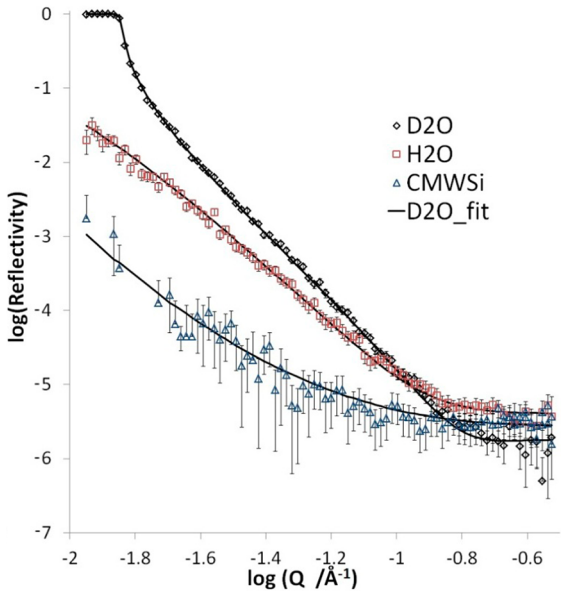

Figure 2. Reflectivity data of bare silicon wafers with three contrasts of water (D_2O, H_2O, and CMWSi). Solid lines are fits data with a surface roughness of 2 ± 1 Å and a 15 ± 3 Å oxide layer with a roughness of 2 ± 1 Å.

are in very good agreement with many other studies of Si wafers by neutron reflection.

Subsequent adsorption of AOT solutions onto silicon wafers was performed on a freshly cleaned substrate for each sample and its pH. This approach was adopted to avoid any potential contamination sample to sample, particularly from bound Ca^{2+} counterions (Fragnetto, G., personal communication). All the substrate crystals were investigated as described above prior to adsorption with three water contrasts. The measured reflectivity was very similar to that shown in Figure 2 with very similar fitted structural parameters, showing good repeatability.

AOT Adsorption: Effects of Counterion Valency and pH. Neutron reflectivity profiles were measured for hydrogenated NaAOT in D_2O with concentrations of 2.5 mM (CMC[49]) and 5 mM (2 × CMC) at pH 7. As illustrated in Figure 3, the reflectivity profiles with and without the NaAOT in D_2O are identical within the error bars of the data. Hence, we conclude that exposure to the NaAOT (with a monovalent ion, sodium) does not lead to any significant adsorption of the AOT, even at high concentration (twice the CMC). This measurement was repeated with a different silicon crystal and fresh NaAOT sample. Again, no adsorption was observed on either occasion.

In contrast, Figure 4a displays the neutron reflection data from a solution of CaAOT with a concentration of 0.5 mM (CMC[49]) in D_2O on silicon. These data exhibit pronounced differences in reflectivity between the bare substrate and with the CaAOT which clearly indicates pronounced adsorption. This adsorption is interesting given that the absolute concentration of the AOT is much lower in the presence of Ca^{2+} than Na^+, yet significantly more adsorption is observed. The adsorption of CaAOT was also repeated on different silicon wafers, with a different batch of CaAOT and on different instruments on different neutron facilities, and was found to be completely reproducible. Hence, we conclude that there is adsorption of AOT, an anionic surfactant on the negatively

dx.doi.org/10.1021/la400767u | Langmuir 2013, 29, 5520−5527

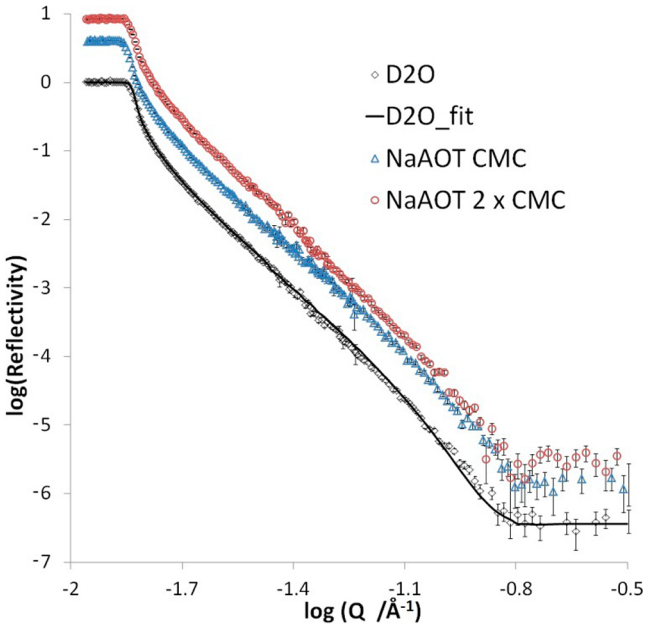

Figure 3. Neutron reflectivity of NaAOT adsorbed on silica at its CMC (2.5 mM) and twice the CMC (5 mM) at pH 7. The reflectivity of the bare silica surface in D_2O is also included. The successive curves are shifted by a factor of 4 for clarity.

charged silica substrate in the presence of divalent, Ca^{2+}, but not monovalent, Na^+.

Figure 4 presents the reflection data from the adsorption of CaAOT at the pHs of 4, 7 and 9, compared to that of the bare silicon wafer. The data at the pH of 4 is essentially unchanged from the bare silicon; hence, we conclude there is no significant adsorption at this low pH. However, at pH 7 and 9, as discussed above, there is significant adsorption.

This variation in adsorption with pH arises from a number of surface and solution equilibria including the variation of silica surface charge with pH. At higher pH, the surface becomes more negative through dissociation of SiOH groups to give more anionic SiO^-. The isoelectric point of silica is usually taken to be low (pH ≈ 2), and the surface gets more negative as the pH increases, although the rate of increase decreases. These anionic surface sites would be able to interact more readily with Ca^{2+} ions. The surface equilibria are discussed further below.

Structure of the Adsorbed Layer. Figure 4 presents the reflection data from the adsorption of CaAOT in two different water contrasts—(a) D_2O and (b) H_2O—used to characterize the CaAOT adsorbed layer. The reflectivity data from both contrasts have been simultaneously fitted to a single structural model, and the fitted parameters are given in Table 2. This data indicates an overall layer thickness of 35 ± 7 Å at pH 7 and of 38 ± 7 Å at pH 9. The extended chain length of a monolayer of the AOT is reported to be ~18 Å;[49,53] hence, we conclude that this adsorbed material is a bilayer. This general behavior is to be expected given that both the solid surface and the surrounding water are hydrophilic and a bilayer structure would avoid unfavorable water−tail interactions.

A single block adsorption model could not fit all the required contrasts, and hence we have used a more complex structural model distinguishing the head and tail regions of the surfactant. This model includes an "inner head" region (close to the solid surface), a "tail region", and an "outer head" layer. The fitted parameters suggest a reasonably complete monolayer adjacent

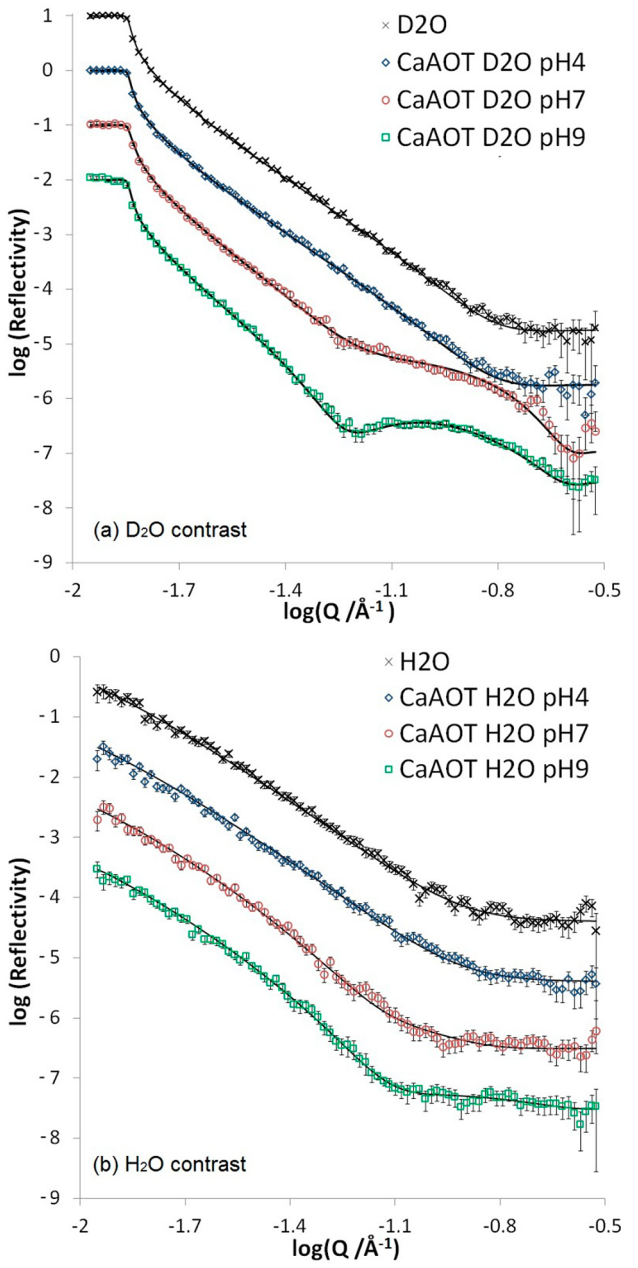

Figure 4. Reflectivity data for solutions of CaAOT on silica at its CMC (0.5 mM) in (a) D_2O and (b) H_2O at the pHs of 4, 7, and 9. Simultaneous fits (solid lines) of the bilayer model to the measured data are also included. The successive curves are shifted by a factor of 10 for clarity.

to the solid surface with 40 vol % water at pH 7 and 60 vol % water at pH 9 in the inner head region. The tail region has less water at both pHs. The outer head layer of the bilayer is somewhat more disordered and rather thicker with more water than the inner head region. The hydrophobic tail region has a thickness of 17 ± 1 and 18 ± 1 Å at pH 7 and 9, respectively, which indicates that the surfactant tails in the bilayer interdigitate. The effective area per pair of AOT molecules in the adsorbed material is approximately 70 ± 5 $Å^2$ at pH 7 and 74 ± 5 $Å^2$ at pH 9, in good agreement with 78 $Å^2$ reported previously at the air/water interface.[49,53] Here we have considered the area per pair of molecules in this comparison as we have a bilayer and the air/water interface has an adsorbed

dx.doi.org/10.1021/la400767u | Langmuir 2013, 29, 5520−5527

Table 2. Fitted Parameters Used To Model the Adsorbed Bilayer of CaAOT[a]

layer	pH	thickness/Å	$\varphi_{water} \pm 0.05$	roughness/Å	area per molecule[b]/Å^2	Γ/μmol·m^{-2}
outer heads	7	11 ± 5	0.85	10 ± 2	70 ± 5	2.4 ± 0.5
tails		17 ± 1	0.10	5 ± 1		
inner heads		7 ± 1	0.4	1 ± 2		
outer heads	9	12 ± 5	0.82	10 ± 2	74 ± 5	2.2 ± 0.5
tails		18 ± 1	0.20	2 ± 1		
inner heads		8 ± 1	0.60	3 ± 1		

[a]φ is the volume fraction of water in the layer, and Γ is the surface excess of CaAOT surfactants. [b]Note that a molecule here is one anionic AOT.

monolayer. Hence, the true area per molecule is half of this value, i.e., 35 Å^2 at pH 7 and 37 Å^2 at pH 9.

The surface excess of CaAOT is found to be 2.4 ± 0.5 μmol·m^{-2} for pH 7 and 2.2 ± 0.5 μmol·m^{-2} for pH 9. This indicates that the amount of surfactants adsorbed on the surface was very similar at both these pHs. As outlined above one might have expected more cation bridging at higher pH (with more negatively charged surface). In fact, the surface charge density of silica surface does not change much above pH ∼ 7.[37−39] Figure 5 illustrates a schematic diagram of the CaAOT adsorption on silicon/silica.

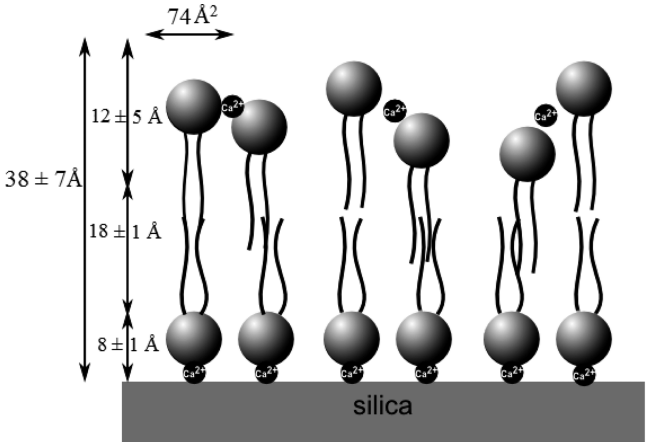

Figure 5. Schematic diagram of adsorbed bilayer of CaAOT on silica at pH 9.

In performing the fit to the reflectivity data, we have to make some estimate of the molecular volume of the calcium AOT. There is clearly significant uncertainty in this process, and the calculated surfactant layer parameters in Table 2 will vary with any misestimation. The volume of NaAOT can be used to provide a crude estimate of the molecular volume of the $Ca(AOT)_2$ which is expected to be roughly twice that of the NaAOT (dominated by the AOT part of the combination). The molecular volume of NaAOT in the bulk crystal (671 Å^3) deduced from the relative molecular mass (444 g·mol^{-1}) and bulk crystal density (1.1 g·cm^{-3}) is taken to represent the closest packing the molecules might reasonably be expected to adopt. Hence, it is expected that the surfactant in the adsorbed layer is somewhat expanded relative to this. Here we have essentially allowed an expansion of ∼10% (to give a molecular volume of ∼730 A^3 per AOT) which is not considered unreasonable to allow for conformational degrees of freedom on release of the molecule from the crystal lattice. Once we have the overall molecular volume, there is also some uncertainty over the apportionment of the molecular volume between the "heads" and "tail" regions in the layer. The total number of tail parts of CaAOT in the bilayer is the same as the total number of inner and outer head parts.

Concentration Behavior. Figure 6 illustrates the variation of the CaAOT reflection with concentration. Interestingly, we

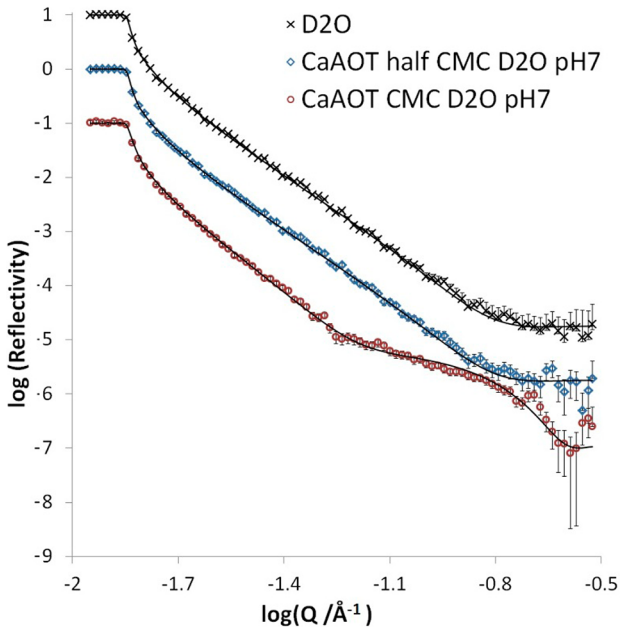

Figure 6. Concentration dependence of CaAOT adsorption at pH 7 in D_2O. The successive curves are shifted by a factor of 10 for clarity.

note that there is rather little change in adsorption at half the CMC (0.25 mM) compared to the bare surface. It is only at the CMC (0.5 mM) that a significant change in reflection, and hence, adsorption is found. This behavior suggests that the self-aggregation of the surfactant might be a significant aspect of the adsorption behavior. The adsorption of the Na-AOT remains low even at twice the CMC of the Na-AOT (see Figure 3) as discussed above. The adsorption onto a hydrophilic surface has been reported to be cooperative and hence switches on sharply at the CMC.[54]

ATR-IR. Figure 7 presents the ATR-IR data from the silicon IRE in NaAOT solution at the CMC (2.5 mM) at pH 9 and the silicon IRE in CaAOT solution at the CMC (0.5 mM) at pH 7, 8, and 9. The data present the region of the spectra where we expect to see C−H vibrations from the alkyl groups in the AOT when adsorbed on the surface, as detailed in Table 3.

The spectrum from the NaAOT at pH 9 does not show any C−H vibrations. Hence, we conclude that here is no significant adsorption of NaAOT under these conditions. This is in excellent agreement with the reflection data above. However, as indicated in Figure 7, there is a significant change in the spectra and hence enhanced adsorption of the CaAOT at pH 8 and 9

dx.doi.org/10.1021/la400767u | Langmuir 2013, 29, 5520−5527

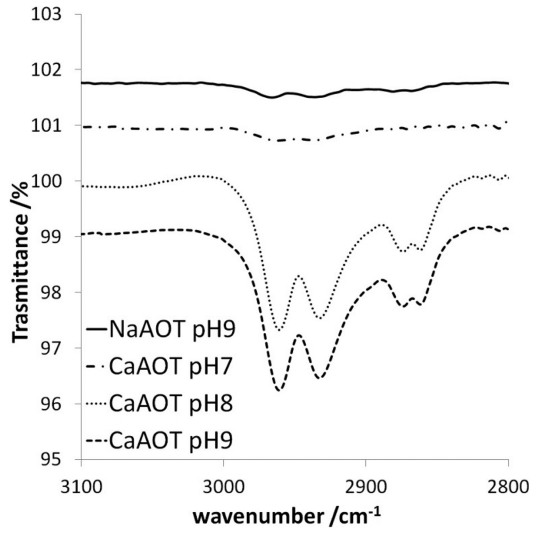

Figure 7. ATR-IR spectra for NaAOT (CMC: 2.5 mM) at pH 9 and CaAOT (CMC: 0.5 mM) at pH 7, 8, and 9 on silicon (100) crystal faces. Each data set was multiplied by a scale factor for clarity.

Table 3. Wavenumbers for Characteristic Bands in the ATR-IR Spectra

wavenumber/cm^{-1}	functional group	vibration mode
~2970	$-CH_3$	antisymmetric
~2930	$-CH_2$	antisymmetric
~2880	$-CH_3$	symmetric
~2860	$-CH_2$	symmetric

that is not observed for the NaAOT. This is also in good agreement with the neutron data above.

Interestingly, ATR-IR data at pH 7 do not show significant CaAOT adsorption. This is somewhat different from the neutron data above where significant adsorption was observed at pH 7. Extensive repeats of the experiment have all shown this behavior. Both ATR and neutrons show the same broad pH dependence with no adsorption at low pH and significant adsorption at high pH. There does however seem to be a subtle difference in the pH at which the adsorption becomes significant. At present, we attribute this difference to the difference in the silicon crystals used for ATR-IR which have a different crystal phase (100 faces) and slightly higher surface roughness (<1 nm) than the neutron reflection crystals (111 faces, 2 Å roughness). In addition, we note there is some small level of uncertainty in the measured pH of the solutions (estimated to be ~0.5 pH units). We have also considered kinetic issues, given that the neutron reflection experiments are relatively slow. However, even after waiting a significant time, the ATR-IR data did not show adsorption when the reflection data did. There is still some uncertainty over the origin of this small difference.

DISCUSSION

The surface charge of silica is pH-dependent, becoming more negative with increasing pH. At pH 4, the surface charge is rather low and becomes more negative with increasing pH. This surface can be modeled by appropriate equilibrium constants.[55] Hence, if the electrostatic repulsion was the main reason inhibiting adsorption, then one might expect a low charged surface (low pH) would have higher adsorption. This is not the case here, where both neutron and ATR-IR do not show any evidence of adsorption.

Another possible mechanism of AOT binding is by the ligand exchange of the surface hydroxyl (−OH) groups by the anionic ligands AOT.[55] This mechanism usually has rather distinctive pH behavior as the number of OH and AOT ions compete at high pH. Hence, the AOT ligand would be expected to exhibit a maximum in adsorption with pH. Again this behavior is not observed. Calculations also indicate that having a high ionic strength cannot be the controlling factor as the CaAOT shows adsorption while the NaAOT does not with ionic strengths of 1.5×10^{-3} and 5×10^{-3} M, respectively.

Another possibility is cation-bridging where divalent ions bind the AOT to the surface silica. The fact that sodium and calcium behave so differently clearly implicates the ion valency as having a principal role in the adsorption although we have already ruled out simple ionic strength effects, as outlined above. The binding of a cation to the silicon surface is expected to increase with pH as more negative surface groups are produced. Indeed, simple equilibrium models of the Si−OH dissociation combined with divalent cation-bridging to these sites suggest the optimal conditions for adsorption by bridging increase with pH, as observed. Therefore, we tentatively conclude that the mechanism of the CaAOT adsorption here is "cation-bridging".

Adsorption of anionic surfactants onto anionic surfaces has been reported in the presence of a nonionic cosurfactant[56] and onto hydrophilic cellulose which is anionic.[57] Similar adsorption was also reported in colloidal systems.[58] Calcium induced adsorption was also reported for zwitterionic surfactants both experimentally[59] and theoretically.[60]

Charge reversal on adsorption of different materials can also be considered as a step toward ion bridging—the reversal of the surface change makes the surface attractive to a like charged additive. This inversion relatively well-known with multivalent ions and polyelectrolytes and forms the basis of layer by layer deposition of polyelectrolyte multilayers. It has also been shown to modify surfactant adsorption.[61−64]

CONCLUSION

In this work we present neutron reflection and ATR-IR evidence for the somewhat unexpected adsorption of a negative surfactant on a negative surface. This adsorption is only found to occur to a significant extent in the presence of divalent calcium ions. The adsorption increases at high pH. In contrast, there is essentially no adsorption in the presence of monovalent sodium ions. One possible explanation of this behavior is "cation-bridging".

AUTHOR INFORMATION

Corresponding Author

*E-mail: stuart@bpi.cam.ac.uk.

Notes

The authors declare no competing financial interest.

ACKNOWLEDGMENTS

We thank BP for financial support for this work and the ILL (9-12-301) and ISIS (RB 1220272) staff and scientists for the allocation of beam time and technical assistance with the NR measurements. We thank Nicholas Parkes for helpful discussions.

REFERENCES

(1) Gao, Y.; Du, J.; Gu, T. Hemimicelle formation of cationic surfactants at the silica gel-water interface. *J. Chem. Soc., Faraday Trans. 1* **1987**, *83* (8), 2671−2679.

(2) Biswas, S. C.; Chattoraj, D. K. Kinetics of adsorption of cationic surfactants at silica-water interface. *J. Colloid Interface Sci.* **1998**, *205* (1), 12−20.

(3) Paria, S.; Khilar, K. C. A review on experimental studies of surfactant adsorption at the hydrophilic solid-water interface. *Adv. Colloid Interface Sci.* **2004**, *110* (3), 75−95.

(4) Fan, A.; Somasundaran, P.; Turro, N. J. Adsorption of alkyltrimethylammonium bromides on negatively charged alumina. *Langmuir* **1997**, *13* (3), 506−510.

(5) Atkin, R.; et al. Mechanism of cationic surfactant adsorption at the solid-aqueous interface. *Adv. Colloid Interface Sci.* **2003**, *103* (3), 219−304.

(6) Franchi, M.; Ferris, J. P.; Gallori, E. Cations as mediators of the adsorption of nucleic acids on clay surfaces in prebiotic environments. *Origins Life Evol. Biosph.* **2003**, *33* (1), 1−16.

(7) Thorarinn, S.; Arnarson, R. G. K. Mechanisms of pore water organic matter adsorption to montmorillonite. *Mar. Chem.* **2000**, *71*, 309−320.

(8) Buckley, J. S.; Liu, Y. Some mechanisms of crude oil/brine/solid interactions. *J. Petrol. Sci. Eng.* **1998**, *20* (3), 155−160.

(9) Lager, A.; et al. Low salinity oil recovery - An experimental investigation. *Petrophys* **2008**, *49* (1), 28−35.

(10) Lee, S. Y.; et al. Low salinity oil recovery − Increasing understanding of the underlying mechanisums. *SPE* **2010**, 129722.

(11) Israelachvili, J. N. *Intermolecular and Surface Forces*, 3rd ed.; Elsevier Inc.: Amstersdam, 2011.

(12) Abraham, T.; et al. Polyelectrolyte-mediated interaction between similarly charged surfaces: Role of divalent counter ions in tuning surface forces. *Langmuir* **2001**, *17* (26), 8321−8327.

(13) Berg, J. M.; Claesson, P. M.; Neuman, R. D. Interactions between mica surfaces in sodium polyacrylate solutions containing calcium ions. *J. Colloid Interface Sci.* **1993**, *161* (1), 182−189.

(14) Pashley, R. M.; Israelachvili, J. N. DLVO and hydration forces between mica surfaces in Mg^{2+}, Ca^{2+}, Sr^{2+}, and Ba^{2+} chloride solutions. *J. Colloid Interface Sci.* **1984**, *97* (2), 446−455.

(15) Pantina, J. P.; Furst, E. M. Colloidal aggregate micromechanics in the presence of divalent ions. *Langmuir* **2006**, *22* (12), 5282−5288.

(16) Zohar, O.; Leizerson, I.; Sivan, U. Short range attraction between two similarly charged silica surfaces. *Phys. Rev. Lett.* **2006**, *96* (17), 177802.

(17) Popa, I.; et al. Attractive electrostatic forces between identical colloidal particles induced by adsorbed polyelectrolytes. *J. Phys. Chem. B* **2009**, *113* (25), 8458−8461.

(18) Besteman, K.; et al. Direct observation of charge inversion by multivalent ions as a universal electrostatic phenomenon. *Phys. Rev. Lett.* **2004**, *93* (17), 170802.

(19) Shklovskii, B. I. Screening of a macroion by multivalent ions: Correlation-induced inversion of charge. *Phys. Rev. E* **1999**, *60* (5), 5802−5811.

(20) Faraudo, J.; Travesset, A. The many origins of charge inversion in electrolyte solutions:effects of discrete interfacial charges. *J. Phys. Chem. C* **2006**, *111* (2), 987−994.

(21) Grosberg, A. Y.; Nguyen, T. T.; Shklovskii, B. I. Colloquium: The physics of charge inversion in chemical and biological systems. *Rev. Mod. Phys.* **2002**, *74* (2), 329.

(22) Nguyen, T. T.; Grosberg, A. Y.; Shklovskii, B. I. Screening of a charged particle by multivalent counterions in salty water: Strong charge inversion. *J. Chem. Phys.* **2000**, *113* (3), 1110−1125.

(23) Terao, T.; Nakayama, T. Charge inversion of colloidal particles in an aqueous solution: Screening by multivalent ions. *Phys. Rev. E* **2001**, *63* (4), 041401.

(24) Lyklema, J. Overcharging, charge reversal: Chemistry or physics? *Colloids Surf., A* **2006**, *291* (1−3), 3−12.

(25) Besteman, K.; van Eijk, K.; Lemay, S. G. Charge inversion accompanies DNA condensation by multivalent ions. *Nat. Phys.* **2007**, *3* (9), 641−644.

(26) Sabbagh, I.; Delsanti, M. Solubility of highly charged anionic polyelectrolytes in presence of multivalent cations: Specific interaction effect. *Eur. Phys. J. E: Soft Matter Biol. Phys.* **2000**, *1* (1), 75−86.

(27) Solis, F. J.; de la Cruz, M. O. Collapse of flexible polyelectrolytes in multivalent salt solutions. *J. Chem. Phys.* **2000**, *112* (4), 2030−2035.

(28) Widom, J.; Baldwin, R. L. Cation-induced toroidal condensation of DNA: Studies with $Co^{3+}(NH_3)_6$. *J. Mol. Biol.* **1980**, *144* (4), 431−453.

(29) Bloomfield, V. A. DNA condensation. *Curr. Opin. Struct. Biol.* **1996**, *6* (3), 334−341.

(30) Zhang, F.; et al. Reentrant condensation of proteins in solution induced by multivalent counterions. *Phys. Rev. Lett.* **2008**, *101* (14), 148101−148104.

(31) Zhang, F.; et al. Universality of protein reentrant condensation in solution induced by multivalent metal ions. *Proteins: Struct, Funct. Bioinf.* **2010**, *78* (16), 3450−3457.

(32) Zhang, F.; et al. Novel approach to controlled protein crystallization through ligandation of yttrium cations. *J. Appl. Crystallogr.* **2011**, *44* (4), 755−762.

(33) Kosmulski, M. The pH-dependent surface charging and the points of zero charge. *J. Colloid Interface Sci.* **2002**, *253*, 77−87.

(34) Kosmulski, M. *Chemical Properties of Material Surfaces*; Marcel Dekker, Inc.: New York, 2001; pp 65−715.

(35) Lin, X. Y.; Farhi, E.; Arribart, H. Determination of the isoelectric point of planar oxide surfaces by a particle adhesion method. *J. Adhes.* **1995**, *51*, 181−189.

(36) Iler, R. K. *The Chemistry of Silica: Solubility, Polymerisation, Colloid and Surface Properties and Biochemistry of Silica*; Wiley-Interscience: New York, 1979.

(37) Bolt, G. H. Determination of the charge density of silica sols. *J. Phys. Chem.* **1957**, *61* (9), 1166−1169.

(38) Milonjic, S. K. Determination of surface ionization and complexation constants at colloidal silica/electrolyte interface. *Colloids Surf.* **1987**, *23* (4), 301−312.

(39) Behrens, S. H.; Grier, D. G. The charge of glass and silica surfaces. *J. Chem. Phys.* **2001**, *115* (14), 6716−6721.

(40) Jauregi, P.; Gilmour, S.; Varley, J. Characterisation of colloidal gas aphrons for subsequent use for protein recovery. *Chem. Eng. J.* **1997**, *65* (1), 1−11.

(41) Penfold, J.; Thomas, R. K. The application of the specular reflection of neutrons to the study of surfaces and interfaces. *J. Phys.: Condens. Matter* **1990**, *2*, 1369−1413.

(42) Born, M.; Wolf, E. *Principles of Optics: Electromagnetic Theory of Propagation, Interference and Diffraction of Light*, 7th ed.; Pergamon Press: Oxford, 1999; p 70.

(43) Harrick, N. J. *Internal Reflection Spectroscopy*; John Wiley & Sons: New York, 1967; pp 1−83, 179−213.

(44) Ekgasit, S.; Ishida, H. New optical depth-profiling technique by use of the multiple-frequency approach with single ATR FT-IR spectrum: Theoretical development. *Appl. Spectrosc.* **1997**, *51*, 1488−1495.

(45) Chan, K. L. A.; Kazarian, S. G. Attenuated total reflection fourier transform infrared imaging with variable angles of incidence. *Appl. Spectrosc.* **2007**, *61*, 48−54.

(46) Leewis, C. M.; Kessels, W. M. M.; de Sanden, M.; van de Sanden, M. C. M.; Niemantsverdriet, J. W. Attenuated total reflection infrared spectroscopy for studying adsorbates on planar model catalysts. *J. Vac. Sci. Technol., A* **2006**, *24*, 296−304.

(47) Daimay, L. V. *The Handbook of Infrared and Raman Characteristic Frequencies of Organic Molecules*; Academic Press: New York, 1991.

(48) Eastoe, J.; et al. Variation of surfactant counterion and its effect on the structure and properties of Aerosol-OT-based water-in-oil microemulsions. *J. Chem. Soc., Faraday Trans.* **1992**, *88* (3), 461−471.

(49) Li, Z. X.; Lu, J. R.; Thomas, R. K. Neutron reflectivity studies of the adsorption of Aerosol-OT at the air/water interfaces: The surface excess. *Langmuir* **1997**, *13*, 3681−3685.
(50) Cubitt, R.; Fragneto, G. D17: the new reflectometer at the ILL. *Appl. Phys. A: Mater. Sci. Process.* **2002**, *74* (1), 329−331.
(51) Webster, J.; Holt, S.; Dalgliesh, R. INTER the chemical interfaces reflectometer on target station 2 at ISIS. *Phys. B: Condens. Matter* **2006**, *385*−*86*, 1164−1166.
(52) Hughes, A. RasCAL, 2012, available at http://sourceforge.net/projects/rscl/.
(53) Fragneto, G.; Li, Z. X.; Thomas, R. K.; Rennie, A. R.; Penfold, J. A neutron reflectivity reflectivity study of the adsorption of Aerosol-OT on self-assembled monolayers on silicon. *J. Colloid Interface Sci.* **1996**, *178*, 531−53.
(54) Tiberg, F.; Joensson, B.; Tang, J.-a.; Lindman, B. Ellipsometry studies of the self-assembly of nonionic surfactants at the silica-water interface: equilibrium aspects. *Langmuir* **1994**, *10* (7), 2294−2300.
(55) Stumm, W.; Morgan, J. J. *Aquatic Chemistry: Chemical Equilibria and Rates in Natural Waters*; John Wiley and Sons Ltd.: New York, 1995.
(56) Penfold, J.; Staples, E.; Tucker, I.; Thomas, R. K. Adsorption of mixed anionic and nonionic surfactants at the hydrophilic silicon surface. *Langmuir* **2002**, *18* (15), 5755−5760.
(57) Tucker, I. M.; Petkov, J. T.; Penfold, J.; Thomas, R. K. Interaction of the anionic surfactant SDS with a cellulose thin film and the role of electrolyte and poyelectrolyte. 2. Hydrophilic cellulose. *Langmuir* **2012**, *28* (27), 10223−10229.
(58) Iglesias, G. R.; Wachter, W.; Ahualli, S.; Glatter, O. Interactions between large colloids and surfactants. *Soft Matter* **2011**, *7* (10), 4619−4622.
(59) Hu, X.; Li, Y.; Sun, H.; Song, X.; Li, Q.; Cao, X.; Li, Z. Effect of divalent cationic ions on the adsorption behavior of zwitterionic surfactant at silica/solution interface. *J. Phys. Chem. B* **2010**, *114* (27), 8910−8916.
(60) Parsons, D. F.; Ninham, B. W. Charge reversal of surfaces in divalent electrolytes: The role of ionic dispersion interactions. *Langmuir* **2010**, *26* (9), 6430−6436.
(61) Penfold, J.; Tucker, I.; Staples, E.; Thomas, R. K. Manipulation of the adsorption of ionic surfactants onto hydrophilic silica using polyelectrolytes. *Langmuir* **2004**, *20* (17), 7177−7182.
(62) Schneider, C.; Hanisch, M.; Wedel, B.; Jusufi, A.; Ballauff, M. Experimental study of electrostatically stabilized colloidal particles: Colloidal stability and charge reversal. *J. Colloid Interface Sci.* **2011**, *358* (1), 62−67.
(63) Szilagyi, I.; Rosicka, D.; Hierrezuelo, J.; Borkovec, M. Charging and stability of anionic latex particles in the presence of linear poly(ethylene imine). *J. Colloid Interface Sci.* **2011**, *360* (2), 580−585.
(64) Shin, Y. W.; Roberts, J. E.; Santore, M. M. The relationship between polymer/substrate charge density and charge overcompensation by adsorbed polyelectrolyte layers. *J. Colloid Interface Sci.* **2002**, *247* (1), 220−230.